# Small polarons and magnetic antiphase boundaries in $Ca_{2-x}Na_xCuO_2Cl_2$ ($x=0.06,0.12$): Origin of striped phases in cuprates

C. H. Patterson
*School of Physics, Trinity College Dublin, Dublin 2, Ireland*

(Received 14 December 2007; revised manuscript received 27 February 2008; published 31 March 2008)

We report hybrid density functional theory calculations on hole doped $Ca_{2-x}Na_xCuO_2Cl_2$ performed in $4\times4$, $4\sqrt{2}\times4\sqrt{2}$, and $8\times2$ supercells with hole concentrations $x=0.0625$ and $x=0.125$. Holes at the lower concentration form small polarons, in which the hole is mainly localized on four oxygen ions surrounding one copper ion. The polaron is a spin one-half ferromagnetic polaron ($Cu_5O_4$), in which the moment on the central copper ion is parallel to those on the four neighboring copper ions and the moment on the oxygen ions is opposed to that on the copper ions. This is therefore an Emery–Reiter spin polaron rather than a Zhang–Rice singlet. At the higher hole concentration ($x=0.125$), many cuprates form stripes. Hybrid density functional theory calculations on linear chains of spin polarons separated by $4a_0$ show a group of bands localized mainly on the stripe. Spins on neighboring copper ions in the stripe are parallel and so the stripe forms a magnetic antiphase boundary between antiferromagnetically ordered blocks of copper spins. Stripes of this kind, which run in one direction only, may explain recent scanning tunneling microscopy data from $Ca_{2-x}Na_xCuO_2Cl_2$ by Kohsaka *et al.* [Science **315**, 1380 (2007)]. We also consider an ordered spin polaron phase where magnetic antiphase boundaries intersect at right angles. In this case, sets of four copper ions in squares at stripe intersections have parallel spins. This phase may be the $4\times4$ checkerboard pattern reported by Hanaguri *et al.* [Nature (London) **430**, 1001 (2004)].

DOI: 10.1103/PhysRevB.77.094523 PACS number(s): 74.20.Mn, 74.72.−h, 71.27.+a, 71.20.−b

## I. INTRODUCTION

Recent experimental[1–7] and theoretical[8–11] studies of transition metal oxides have emphasized the polaronic character of their hole states. Early models for hole states in copper oxide superconductors, in which the hole was localized chiefly on oxygen ions, include the Zhang–Rice singlet state[12] and the Emery–Reiter spin polaron.[13] More recent first principles studies of hole-doped cuprates, which have found states where holes reside mainly on oxygen ions, include an LDA+$U$ study of $La_{1.88}Sr_{0.12}CuO_4$ (Ref. 10) and quantum chemical studies of clusters representing $CuO_2$ planes in cuprates.[11]

These observations are in sharp contrast to density functional theory studies which omit a Hubbard $U$ term, in which case the antiferromagnetic, insulating parent compound is usually predicted to be metallic.[14,15] An extensive model Hamiltonian study of striped phases of cuprates found linear chains of holes in a half-filled stripe state[16] and the formation of charged lines of holes on oxygen ions in $CuO_2$ planes was predicted using Hubbard models.[17–19]

A hybrid density functional approach,[20,21] which includes Hartree–Fock exchange with a weighting factor, is used to study hole states in $Ca_{2-x}Na_xCuO_2Cl_2$ (Na-CCOC), with $x=0.0625$ and 0.125 in this work; inclusion of Hartree–Fock exchange in the Hamiltonian leads to a polaronic description of hole states in cuprates and other oxides[8,9,22] and correctly predicts an antiferromagnetic insulating state for the parent compound of the doped cuprates studied here.[23] An important feature of the spin-polaron model for a hole state, vis-à-vis the Zhang–Rice singlet state, is that transition metal ions which are adjacent to the polaronic oxygen ion are coupled into a ferromagnetic state by the hole localized on the oxygen ion. This can be explained in terms of a simple double exchange model.[13] Polaronic states of transition metal oxides therefore contain modified spin and charge order compared to the undoped parent compounds.

By using $4\times4$ supercell calculations on $Ca_2CuO_2Cl_2$ (CCOC) with one electron per cell removed or one calcium ion replaced by a sodium ion, we show that isolated, small polarons with repulsive Coulomb interactions form at $x=0.0625$. These are similar to polarons found using quantum chemical methods on clusters.[11] By using $8\times2$ supercell calculations with four electrons per cell removed or four calcium ions substituted by sodium ions, we find that both half-filled $4\times\infty$ stripes of spin polarons and a $4\times4$ checkerboard pattern of intersecting stripes of spin polarons form stable, metallic states at $x=0.125$.

We use these findings to argue that spin-charge stripes in cuprates, which were observed by scanning tunneling microscopy (STM),[24,25] neutron scattering,[26–28] NMR,[29,30] and other experimental techniques,[31] are due to ordered stripes of spin polarons. Since polarons contain ferromagnetically coupled transition metal ion spins, they must order in such a way as to minimize disruption to the antiferromagnetically ordered spins in hole-poor regions. Single, isolated polarons may be accommodated in the antiferromagnetic background of a $CuO_2$ plane without disrupting it; when higher densities of holes have to be accommodated, they can order in one-dimensional (1D) stripes of spin polarons, which are magnetic antiphase boundaries (APBs). The universal nature of stripes in cuprates is illustrated by the fact that common stripe features are observed by scanning tunneling conductance measurements in both Na-CCOC and $Bi_2Sr_2Dy_{0.2}Ca_{0.8}Cu_2O_{8+\delta}$ (Dy-Bi2212).[25]

Further experimental evidence for polaronic states in cuprates is provided by the observation of strong electron-phonon coupling: Very broad, Gaussian photoemission line

 

shapes are widely observed in cuprates and attributed to Franck–Condon broadening;[3,6] pinning of charge carriers by a crystallographic distortion in a low temperature tetragonal phase of $La_{2-x}Ba_xCuO_4$ (LBCO), with $0.11<x<0.14$, can be lifted and superconductivity restored by application of hydrostatic pressure;[1] new features in the midinfrared optical absorption spectrum of doped transition metal oxides, including cuprates,[32,33] were attributed to polarons and modeled using a model Hamiltonian approach.[16] A phonon anomaly was observed in LBCO ($x=0.12$) at a wave vector, which corresponds to the $4a_0$ stripe spacing.[34] $a_0$ is the lattice constant in $CuO_2$ planes.

In the following sections of this paper, we give a brief summary of applications of hybrid density functional calculations to doped transition metal oxides and results of hybrid density functional calculations on Na-CCOC in the low hole-density limit ($x=0.0625$) and at $x=0.125$ where stripes are best formed. Results of calculations on $8\times2$ and $4\sqrt{2}\times4\sqrt{2}$ magnetic unit cells of Na-CCOC with $x=0.125$ and 1D or intersecting stripes are given in the following sections. These results are then discussed in the context of a number of experimental and theoretical data and the paper is summarized in the final section. Details of calculations are given in the Appendix.

## II. HYBRID DENSITY FUNCTIONALS

Hybrid density functionals, whose key feature is that they incorporate combinations of Hartree–Fock exchange and conventional density functional approximations to exchange with weights that sum to unity,[35] are becoming more popular for solid state electronic structure calculations. Experience with a range of oxides[23,36–39] shows that exchange coupling constants are correctly predicted for weights of the Hartree–Fock exchange in the range of 0.3–0.4 (Refs. 37–39) and that the particular choice of conventional density functional approximation used in combination with the Hartree–Fock exchange does not change the predicted values for exchange constants by a large amount.[35] On the other hand, experience shows that band gaps of oxides are more accurately predicted with weights for Hartree–Fock exchange around 0.2.[23,36–41] The Becke-3 Lee–Yang–Parr (B3LYP) hybrid density functional[20,21] contains Hartree–Fock exchange with weight $A$, the local density approximation to exchange $E_x^{LDA}$ (Ref. 42) with weight $(1-A)$, Becke's gradient corrected exchange functional $E_x^{Becke}$ (Ref. 43) with weight $(1-A)B$, the Lee–Yang–Parr approximation to the correlation functional $E_c^{LYP}$ (Ref. 44) with weight $C$, and the Vosko–Wilks–Nusair approximation to the electron correlation functional $E_c^{VWN}$ (Ref. 45) with weight $(1-C)$,

$$E_{xc}=(1-A)(E_x^{LDA}+BE_x^{Becke})+AE_x^{HF}+(1-C)E_c^{VWN}+CE_c^{LYP}. \quad (1)$$

The B3LYP hybrid density functional, with $A=0.2$ and also with $A$ adjusted to 0.4 and $B$ and $C$ fixed at their canonical values, is used throughout this work. A heuristic argument for including a fraction of the Hartree–Fock exchange in the exchange functional is that the dynamically screened Hartree–Fock exchange is included in the $GW$ approximation.[46] The extent of screening can be estimated as the reciprocal of the electronic part of the macroscopic dieletric constant, which is around 5 in many oxides, including the cuprates.[47] Of course, the extent of screening depends on electron or hole energies and it is not uniform in space, as it is in hybrid density functionals. However, a recent calculation on NiO, which used self-consistent wave functions and energy eigenvalues from a B3LYP calculation as a starting point for a $GW$ calculation, resulted in a $GW$ band structure which was very similar to that from the self-consistent B3LYP calculation.[40]

The threshold weight of Hartree–Fock exchange for prediction of a localized hole state in a $4\times4$ supercell lies between $A=0.2$ and 0.3 when the hole is generated by removing an electron and replacing it by a uniform, neutralizing background charge. For values of $A$ below this threshold value, a delocalized hole state is predicted, and above this value, a strongly localized small polaron state is predicted. A similar threshold for localization of a self-trapped exciton was reported[48] in a hybrid density functional calculation on sodium chloride. Localization of holes in manganites[8,9] was previously found using unrestricted Hartree–Fock (UHF) theory ($A=1.0$) or hybrid functionals.[22] UHF theory does not predict the correct $CE$-type magnetic ground state of $La_{0.5}Ca_{0.5}MnO_3$ (Ref. 49); instead it predicts an $A$-type ground state;[8] a hybrid functional calculation with a reduced

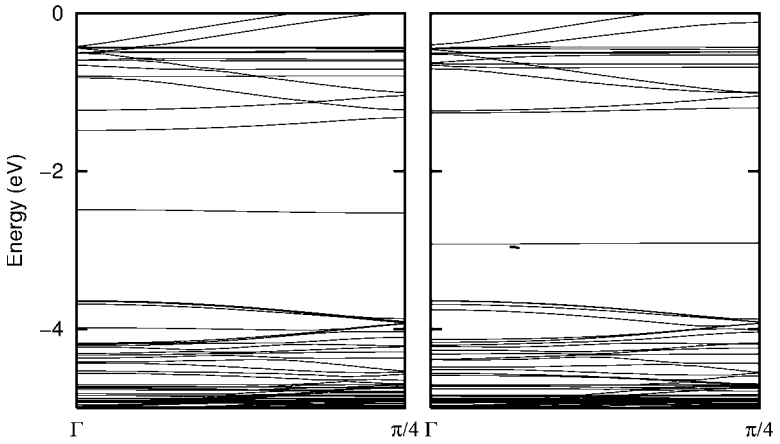


FIG. 1. Minority spin (left panel) and majority spin (right panel) band structures for a $4\times4$ supercell with one localized hole introduced by replacing a calcium ion by a sodium ion. The valence band maximum occurs at −3.6 eV. Dispersionless states are found in the band gap for either spin state. A weakly dispersive occupied state at −4.0 eV in the minority spin band structure is the state where the wave function amplitude is missing from the polaron. Band dispersion is shown parallel to the Cu-O bond direction. The Brillouin zone boundary of the primitive $1\times1$ unit cell occurs at $(\pi,0)$ in the units used for wave vector magnitude.

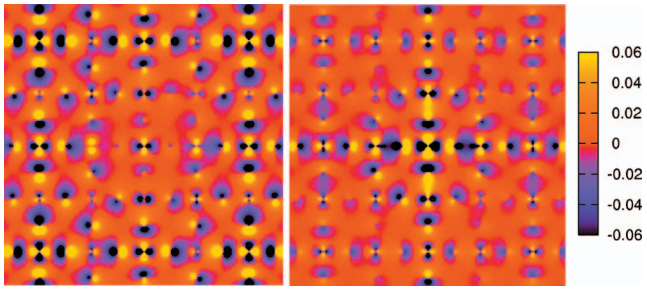


FIG. 2. (Color) Wave function amplitudes at the Γ point of the Brillouin zone for Na-CCOC 4×4 supercell containing one sodium ion. (Left panel) Wave function amplitude for occupied minority spin state at −4.0 eV where amplitude is missing from the polaronic $CuO_4$ unit. (Right panel) Localized minority spin empty state at midgap in Fig. 1. Almost all wave function amplitude is localized on the polaron.

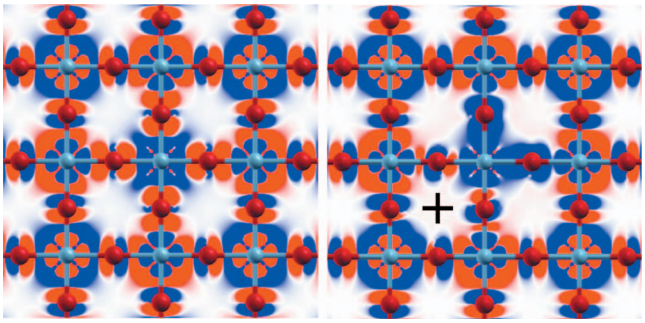

FIG. 3. (Color) Spin densities around polarons formed by removing an electron from the 4×4 supercell (left panel) or by replacing a calcium ion by a sodium ion (right panel). The sodium ion is located just below the + symbol on the $CuO_2$ plane.

weight of Hartree–Fock exchange reverses the energetic ordering of the *CE*- and *A*-type states and predicts the correct ground state.[50]

### III. LOW HOLE-DENSITY LIMIT

Calculations where a single hole was introduced into the supercell were performed on supercells of CCOC containing 32 copper ions in two 4×4 layers. Holes were introduced by removing an electron and adding a uniform background charge to maintain charge neutrality of the unit cell or by replacing a calcium ion by a sodium ion. A localized hole state is obtained in one of the $CuO_2$ layers in the supercell so that the hole density in that layer is 0.0625 per copper ion. If the lattice is allowed to relax, localization of a hole is accompanied by contraction of Cu-O bonds around the copper ion at the center of the hole wave function, i.e., a polaron is formed.

The polaron is confined to one $CuO_4$ unit, judged by perturbations to the charge and spin densities and modulations of bond lengths when all atomic positions in the supercell were relaxed. Formation of the polaron is accompanied by the appearance of dispersionless states in the middle of the band gap (Fig. 1). Localized states appear in the band gap for either spin state because of the Coulombic attraction of the polaronic hole. Minority spin wave functions for the state in the band gap and a filled state near the top of the valence band where the amplitude on the polaron is "missing" are shown in Fig. 2. Very similar pairs of empty and filled states are found when the hole is introduced either by replacing a calcium ion (Fig. 2) or by removing an electron (not shown).

The degree of localization of a polaronic hole depends on the weight of the Hartree–Fock exchange used in a calculation and whether the hole is introduced by removing an electron or replacing a calcium ion by a sodium ion. When the hole is introduced by removing an electron and a hybrid functional with $A=0.9$ is used, the hole localizes on one oxygen ion, which has a moment of $0.60\mu_B$; its sense is opposed those of the magnetic moments on the neighboring copper ions, which each have a moment of $0.85\mu_B$.

The moment on the oxygen ion markedly decreases when $A$ is reduced. With $A=0.4$, the polaron is equally distributed on four oxygen ions surrounding one copper ion. The moment on the central copper ion is $0.60\mu_B$ (Table I), the moments on the other copper ions in the polaron are $0.72\mu_B$, while moments on copper ions in the $CuO_2$ plane which contains no hole are $0.75\mu_B$. Moments on each polaronic oxygen ion are $-0.05\mu_B$ and polaronic oxygen ions have a smaller net charge than other oxygen ions by $0.09e$. When the hole is introduced by removing an electron and $A=0.2$, the hole state is delocalized. However, a localized state does form when $A=0.2$ and the hole is introduced by substituting a calcium ion by a sodium ion. The polaron spontaneously forms on a $CuO_4$ unit next to the sodium ion. Spin densities around a polaron formed either way are compared in Fig. 3. Spin density around the polaron which is formed by removing an electron has fourfold symmetry, while the symmetry of the spin density around the polaron formed by substituting a calcium ion is lowered to a mirror plane perpendicular to the $CuO_2$ plane, owing to the location of the sodium ion.

Magnetic moments on copper and oxygen ions in a polaron generated by substituting a calcium ion by a sodium ion are given in Table I. The central copper ion has a moment of $0.32\mu_B$ while other copper ions in the polaron next to the sodium ion have moments of $0.44\mu_B$ and those away from the sodium ion have moments of $0.49\mu_B$. Copper ions in the $CuO_2$ plane where there is no hole have moments of $0.49\mu_B$. Magnetic moments on oxygen ions in the polaron next to the sodium ion are 0.02, while oxygen ions away from the sodium ion have moments of $0.07\mu_B$ (Table I). These oxygen moments have the same sense as those of the copper ions in the polaron, whereas magnetic moments on oxygen ions in the polaron formed by removing an electron have the opposite sense compared to moments on the copper ions. Localization of the state formed in the band gap, together with the observation of a valence band state where there is missing amplitude on the polaron site, suggests that hole localization is accompanied by the vacated state being pushed into the band gap.

The structure of the polaron introduced by removing an electron from the supercell and with $A=0.4$ was determined by relaxing positions of all ions in the 4×4 supercell. The equilibrium Cu-O bond length in CCOC is 1.93 Å.[23] When the 4×4 supercell is relaxed, the oxygen bond length to the central copper ion in the polaron decreases by 4% to 1.86 Å,

TABLE I. Magnetic moments on copper and oxygen ions in small polarons and stripes in units of $\mu_B$.

| Site | Cu moment ($\mu_B$) | O moment ($\mu_B$) |
|---|---|---|
| | $4\times4$ supercell[a] | |
| Center | 0.32 | |
| Left, below | 0.44 | 0.02 |
| Above, right | 0.49 | 0.07 |
| No hole | 0.51 | 0.00 |
| | $4\times4$ supercell[b] | |
| Center | 0.60 | |
| Nearest neighbor | 0.72 | −0.05 |
| No hole | 0.75 | 0.00 |
| | $8\times2$ supercell[c] | |
| Stripe | 0.51 | −0.06 |
| Antiferromagnetic | 0.52 | −0.01, 0.00 |
| | $4\sqrt{2}\times4\sqrt{2}$ supercell[d] | |
| Square | 0.60 | −0.14 |
| Stripe | 0.57 | −0.13 |
| Antiferromagnetic | 0.55 | 0.00 |

[a]Ca substituted by Na with $A=0.2$. Left, right, above, and below refer to positions of oxygen ions relative to the central copper ion in the polaron, as shown in the right panel of Fig. 3.
[b]Hole generated by removing electron with $A=0.4$.
[c]Holes generated by removing four electrons with $A=0.2$. Stripe refers to copper ions in the APB and oxygen ions in the center of the APB. Antiferromagnetic refers to copper ions between stripes. The oxygen ion adjacent to the stripe copper ion has a nonzero moment.
[d]Holes generated by removing eight electrons with $A=0.2$. Moments given are for copper and oxygen ions within copper ion squares at stripe intersections, stripes between intersections, and antiferromagnetic regions. Moments on oxygen ions connecting squares and stripes or stripes and antiferromagnetic regions are all less than 0.005 in magnitude.

while the oxygen bond lengths to the other copper ions in the polaron increase by 4.1% to 2.01 Å. Changes in other bond lengths in the supercell are all less than 1%. A bond length contraction of 5% around the central copper ion in polarons was found in quantum chemical studies of cuprate clusters.[11] Modulation of bond distances by the polaron is therefore nearly completely confined to the $Cu_5O_4$ central complex of the polaron—it is a small polaron.

Calculations were performed with two holes in a $4\times4$ supercell, with both holes in the same $CuO_2$ plane, in order to determine whether a bipolaron is formed and to discover the repulsive or attractive nature of the interaction of pairs of polarons. No lattice relaxation was performed owing to the high computational cost of such calculations. Four arrangements of polaron pairs in a $4\times4$ supercell were considered (Fig. 4). Three of these have polarons in a staggered arrangement with separations of $\sqrt{2}$, $\sqrt{5}$, or $2\sqrt{2}a_0$ and one is a linear bipolaron with a separation of polaron centroids of $2a_0$. The relative energies of these bipolaron structures are shown in Fig. 5; all arrangements of polaron pairs studied showed repulsive interactions. The linear bipolaron is particularly unstable compared to polarons which are staggered along a diagonal. The most stable configuration is where all polarons in the lattice are maximally separated.

The Coulomb energy of two charges of magnitude $e$ separated by $2a_0$ and screened by a dielectric constant, $\epsilon_\infty=5$, is 360 meV. The charges on polarons in these calculations are repeated in neighboring supercells, rather than interacting as isolated pairs of charges. This calculation does suggest, however, that these small polarons have repulsive Coulomb interactions which are screened by a dielectric constant of order 5. The electrostatic repulsion would of course decrease if the lattice were allowed to relax. The phonon contribution to the dielectric constant of cuprates is around 30 (Ref. 51) and so these repulsive interactions are expected to be significantly reduced by lattice relaxation.

## IV. STRIPE FORMATION HOLE DENSITY

In the previous section we reported calculations which showed that small polarons with repulsive Coulomb interactions form in $CuO_2$ layers for low hole concentrations ($x\leqslant0.125$). Phases known as spin glass states are experimentally observed at the upper end of this range of hole concentrations.[25,52] Closer packing of small polarons at hole concentrations above $x=0.125$ is unlikley, owing to the high energetic cost of their Coulomb repulsions. There have been many experimental reports of stripe formation in cuprates for $x\sim0.125$ and recent data from STM (Ref. 25) and neutron scattering experiments[28,53] show stripe charge and spin den-

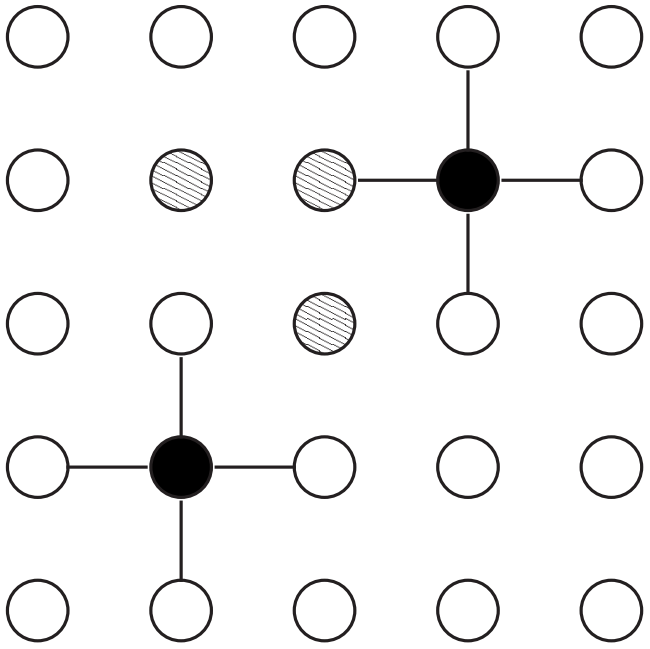

FIG. 4. Relative displacements of small polarons in a $CuO_2$ plane used in the calculations. Two polarons separated by $2\sqrt{2}a_0$ are shown with filled centroids. If the polaron at bottom left is fixed, the other polaron centroids used in calculations are at locations shown as hatched circles.

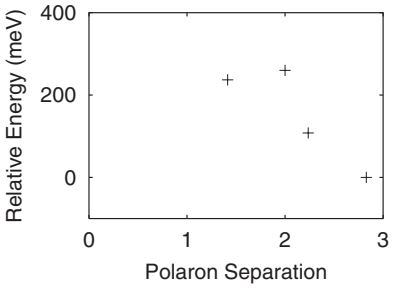


FIG. 5. Relative energies of $4\times4$ supercells containing pairs of polarons with different nearest neighbor separations in units of the $CuO_2$ plane lattice constant.

sity modulations in $CuO_2$ layers which are first observed at lower hole concentration ($x<0.1$) but are generally best observed for $x\sim0.125$. Scanning tunneling conductance measurements in Na-CCOC and Dy-Bi2212 (Ref. 25) clearly show stripes separated by $4a_0$. We propose that the striped phase at $x=0.125$ is composed of chains of Emery–Reiter spin polarons,[13] in which the polaron is localized on a single oxygen ion and its neighboring copper ions.

Polaronic oxygen ions, where a hole is partially localized, favor ferromagnetic double exchange couplings of neighboring metal ions in transition metal oxides, while antiferromagnetic superexchange couplings are favored in undoped oxides. Superexchange is particularly strong in undoped cuprates and is typically around 130 meV.[54] When a certain density of holes is reached, spin polarons are likely to order in a way which accommodates ferromagnetic couplings of copper spins which neighbor polaronic oxygen ions and antiferromagnetic order for copper ions which neighbor other oxygen ions. A stable structure is possible at $x=0.125$ for ordered stripes of spin polarons separated by $4a_0$. Holes are localized on chains of spin polarons which contain oxygen ions whose neighboring copper spins are ferromagnetically coupled [Fig. 6 (top panel)]. They are separated by blocks of antiferromagnetically ordered copper spins where the hole density is small. There is one hole per pair of oxygen ions in the stripe at this hole concentration and stripes exist at magnetic APB. Support for this explanation for stripes in cuprates comes from LDA+$U$ (Ref. 10) and model Hamiltonian calculations.[16]

The schematic diagram in the top panel of Fig. 6 shows blocks of antiferromagnetically ordered copper spins separated by magnetic APB containing polaronic oxygen ions and ferromagnetically ordered copper spins. The spin density obtained from a hybrid DFT calculation with $A=0.2$ and in which holes were introduced into the $8\times2$ supercell by removing electrons is shown in the middle panel of Fig. 6. Note that these spin polarons spontaneously form at $A=0.2$ at this hole concentration, whereas small polarons at lower hole concentration only formed when the hole was introduced by substituting a calcium ion by a sodium ion at $A=0.2$. The electronic band structure for this phase is shown in Fig. 7(a) and the Brillouin zone of the $8\times2$ supercell is superposed on the Brillouin zone for the $1\times1$ primitive cell in Fig. 7(b). This is a metallic state and the band structure around the Fermi energy shows a group of four nearly de-

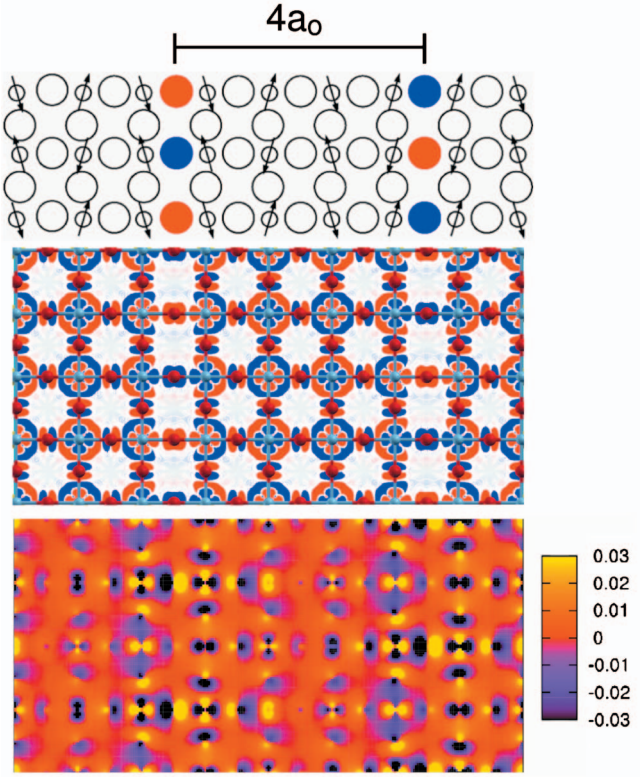


FIG. 6. (Color) Hybrid DFT wave function amplitudes and spin density of stripes formed by magnetic APB. (Top panel) Schematic illustration of spin order in an $8\times2$ supercell. Oxygen ions (large circles) at the centers of APB are colored red or blue according to their net spin density, and spins on copper ions (small circles) are indicated by arrows. (middle panel) Spin density in a $CuO_2$ plane in two $8\times2$ supercells from a hybrid DFT calculation. Copper ions are shown as gray spheres and oxygen ions as red spheres. Red and blue filled regions show where spin density exceeds $\pm0.0005\mu_B$ Bohr$^{-3}$. (Bottom panel) Filled state electronic wave function amplitude at the $\Gamma$ point of the Brillouin zone. Each panel is to the same scale.

generate bands which cross the Fermi energy at around $k=\pi/4$ along the stripe direction. There is very little dispersion of these bands in the direction perpendicular to the stripes and there is one such half-filled "stripe band" per stripe in the supercell. The wave function for one of the

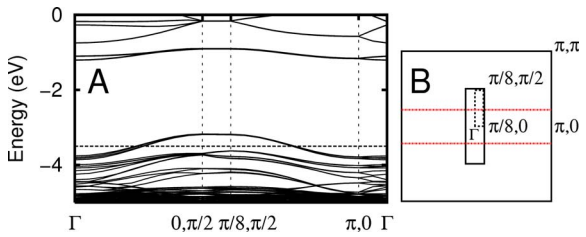


FIG. 7. (Color online) (A) Hybrid DFT electronic band structure and (B) Brillouin zone for an $8\times2$ supercell (small rectangle) superposed onto the Brillouin zone for the $1\times1$ primitive unit cell (large square). The Fermi energy in the band structure is marked by a horizontal line in part (A) and by a pair of horizontal lines in part (B). The absolute values of energy band eigenvalues are shown.

stripe bands at the Γ point of the Brillouin zone is shown in the bottom panel of Fig. 6. Modulation of the wave function amplitude from cell to cell along the stripe is caused by alternation of spins on neigboring spin polarons. Wave functions corresponding to this group of bands are strongly localized on the Cu-O-Cu units which form the stripe and the orbital shape resembles the Wannier function for the stripe bands obtained in an LDA+$U$ calculation.[10] Filled and vacant states localized in the antiferromagnetic regions between the stripes lie below and above the filled and vacant states (Fig. 7) localized on the stripe Cu-O-Cu chains. Stripe regions are therefore metallic, while antiferromagnetic regions between them are not.

Mulliken charge populations on copper and oxygen ions in the stripe and in antiferromagnetic regions differ by only $0.005e$ (copper ions) or $0.015e$ (oxygen ions); hence, although the stripe band contains holes, net charges on ions within and between stripes are almost the same. Magnetic moment magnitudes on copper ions along the APB are $0.51\mu_B$ compared to $0.52\mu_B$ in the intervening antiferromagnetic regions (Table I and $0.56\mu_B$ in a hybrid DFT calculation with $A=0.2$ on undoped CCOC).[23] An LDA+$U$ calculation on stripes in $La_{1.88}Sr_{0.12}CuO_4$ found magnetic moments of $0.74\mu_B$ and $0.67\mu_B$ on copper ions in APB and between APB, respectively.[10] There is a small magnetic moment of magnitude $0.06\mu_B$ on each oxygen ion in the center of the APB, which is opposed in sense to the copper ion moments. The moment alternates in sign along the APB, as shown by the changing color of the spin density along the chain (Fig. 6). Oxygen ions just outside the APB have small magnetic moments ($0.01\mu_B$) and the oxygen ion in the center of the antiferromagnetic region is zero by symmetry.

## V. 4×4 CHECKERBOARD PATTERN STATE

The first scanning tunneling conductance measurements of $4a_0$ period stripes in Na-CCOC[24] showed a 4×4 modulation of the conductance of $CuO_2$ layers in a structure, which was described as a checkerboard pattern where 4×4 "tiles" fill $CuO_2$ planes. However, a more recent study by the same group found a one-dimensional stripe state with stripes separated by $4a_0$.[25] These scanning tunneling conductance measurements are performed in a way that is not sensitive to spin orientation and so only the charge periodicity is observed in the experiment.

The stability of intersecting APB's which have a 4×4 charge unit cell was investigated by performing hybrid DFT calculations on a $4\sqrt{2}\times4\sqrt{2}$ supercell. If 1D stripes consist of magnetic APB separated by antiferromagnetic regions of width $4a_0$, then the 4×4 tiles that make up the checkerboard pattern are likely to consist of coherent intersections of 1D stripes, where magnetic ordering on stripes of either orientation is related. Since holes localized in magnetic APB induce magnetic moments on neighboring copper ions to be oriented parallel to one another, a *quadruple* of copper ions at a stripe intersection must have its spins aligned parallel (Fig. 8). Since tiles in the checkerboard pattern have a width of $4a_0$, spin orientations of copper ion quadruples must alternate every $4a_0$ along either stripe direction to allow antiferromagnetic coupling of all spins in a 4×4 block of spins confined by magnetic APB. This results in the $4\sqrt{2}\times4\sqrt{2}$ magnetic unit cell, as schematically shown in the top left panel of Fig. 8.

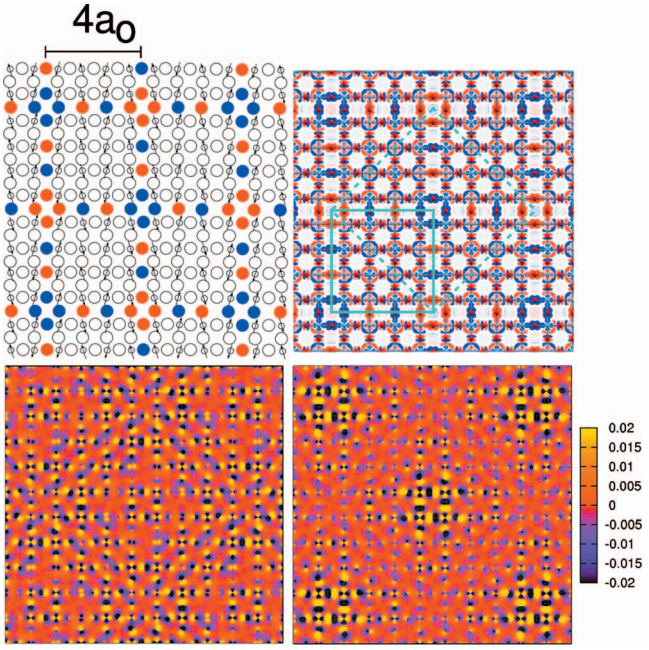


FIG. 8. (Color) Spin density and hybrid DFT wave function amplitude in a $4\sqrt{2}\times4\sqrt{2}$ tile supercell. (Top left panel) Schematic illustration of spin order in a $4\sqrt{2}\times4\sqrt{2}$ supercell. Oxygen ions (large circles) at the centers of APB are colored red or blue according to their net spin density, and spins on copper ions (small circles) are indicated by the arrows. (top right panel) Spin density in a $CuO_2$ plane in $4\sqrt{2}\times4\sqrt{2}$ supercells from a hybrid DFT calculation. The boundary of the $4\sqrt{2}\times4\sqrt{2}$ spin density unit cell is marked by a blue dotted line and the boundary of the 4×4 charge density unit cell is marked by a solid blue line. Copper ions are shown as gray spheres and oxygen ions as red spheres. The red and blue filled regions show where the spin density exceeds $\pm0.0005\mu_B$ Bohr$^{-3}$. (Bottom left panel) Electronic wave function amplitude in $CuO_2$ planes for the highest energy filled state at Γ point and (Bottom right panel) the lowest energy vacant state at Γ point of the Brillouin zone. All parts of the figure are to the same scale.

The spin density from a hybrid DFT calculation on a $4\sqrt{2}\times4\sqrt{2}$ magnetic unit cell is shown in the top right panel of Fig. 8. Holes were introduced by removing eight electrons from the supercell, which contained 64 copper ions. The dotted blue line shows the magnetic unit cell and the solid blue line shows the charge unit cell. Magnetic moments on Cu-O-Cu units in 1D stripes alternate with period $2a_0$ along the stripe, but in the tile structure, magnetic moments on Cu-O-Cu units alternate with period $8a_0$, because the stripe intersection breaks the period-2 alternation in a 1-D stripe. The spin density from the hybrid DFT calculation closely resembles that in the schematic diagram in Fig. 8.

The hybrid DFT band structure for the $4\sqrt{2}\times4\sqrt{2}$ supercell is shown in Fig. 9. The Fermi level is located in a group of bands around −3.4 eV and a state at the Fermi energy is shown in the bottom left panel of Fig. 8. There is a doubly degenerate dispersionless state at −2.9 eV whose wave func-

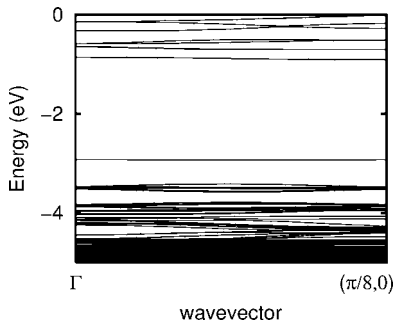


FIG. 9. Hybrid DFT electronic band structure for $4\sqrt{2}\times 4\sqrt{2}$ supercell. The band dispersion is shown parallel to the CuO bond direction. The Brillouin zone boundary of the primitive $1\times 1$ unit cell occurs at $(\pi,0)$.

tion amplitude is shown in the bottom right panel of Fig. 8. Hybrid DFT wave function amplitudes for the highest energy filled state and a vacant state in the band gap at the Γ point of the Brillouin zone are shown in the bottom panels of Fig. 8. The filled state shown occurs at the Fermi level and its wave function shows a similar localization pattern to that found in the 1D striped phase in Fig. 6, where it is mainly on Cu-O-Cu units of one spin orientation in magnetic APB. The vacant state lies in the band gap ~0.5 eV above the Fermi energy and is strongly localized at APB intersections.

Net charges on copper and oxygen ions are nearly uniform in $4\sqrt{2}\times 4\sqrt{2}$ intersecting stripes; the range of net charges on copper ions is only $0.013e$ and that on oxygen ions is $0.030e$. Magnetic moments on copper ions were $0.60\mu_B$, $0.57\mu_B$, and $0.55\mu_B$ in square quadruples of copper ions at stripe intersections, copper ions in stripes between squares, and in antiferromagnetic regions, respectively (Table I). There are quite large magnetic moments on oxygen ions located within copper quadruples $(0.14\mu_B)$ and in stripes $(0.13\mu_B)$, whereas moments on oxygen ions in antiferromagnetic regions are very small.

## VI. DISCUSSION

### A. Limitations of mean field approaches

We begin this section by considering limitations of mean field approaches for treating strongly correlated electron systems. The greatest limitation of conventional density functional methods, when applied to insulating transition metal oxides, is their tendency to predict them to be metallic.[14,15] This limitation is removed either by using the LDA+$U$ approach, in which a Hubbard $U$ term is added to the density functional Hamiltonian, or by adding a Hartree–Fock exchange term to the Hamiltonian, as is done in the hybrid density functional methods used in this work. As noted above, the B3LYP functional used in this work correctly predicts the undoped compound, CCOC, to be an antiferromagnetic insulator.[23] However, conventional density functional methods predict Fermi surfaces of overdoped cuprates quite accurately when the doping level is high enough to produce a fairly good metal.[55] Thus, we expect methods such as hybrid density functionals or LDA+$U$ to give a good description of low doped systems when screening is limited and the electronic structure can be described by a single electronic configuration. Increased doping results in greater screening of the Hartree–Fock exchange and the electronic structure around the Fermi energy is well described by conventional density functionals.

Mean field methods are not capable of treating situations where there are strong fluctuations between electronic configurations. For example, long range antiferromagnetic order, which is observed in undoped cuprate compounds, is rapidly destroyed by doping, even at doping levels as low as $x=0.02$.[52] This could be caused by motion of small polarons leaving a temporary wake of disordered magnetic moments, creation of noncolinear magnetic moments over some range about a small polaron, or a lattice populated by disordered polaron-ferron magnetic moments—a spin glass. Any of these effects would destroy long range antiferromagnetic order and none of them is described by a mean field wave function of the type reported in Sec. III.

Stripes in cuprates are believed to exist either as fluctuating or static stripes.[31] Pinning of stripes to the lattice depends on the strength of the electron-phonon coupling. Experimental evidence from transport measurements,[1] STM,[24,25] and neutron and x-ray scattering[28,34,53,63] shows that a long range order is frozen to the lattice in a wide range of doped cuprates. Obviously, mean field methods are restricted to a single electronic configuration and can only describe static stripes.

Finally, mean field methods cannot describe the singlet spin fluctuations which are present in the Zhang–Rice singlet.[12] The latter contains two configurations, in which spins of opposite orientation are localized on copper and oxygen ions and are superimposed with a minus sign. Single electronic configuration mean field methods such as those used here only contain one of these configurations. These methods therefore omit the resonance stabilization of the Zhang–Rice singlet state which arises from a pair of configurations. However, this energy is expected to be relatively small. The Zhang–Rice singlet model only includes one copper ion and four neighboring oxygen ions and therefore omits coupling between the central copper ion and its four copper neighbors. It does not predict whether a hole localized on four oxygen ions around a central copper ion has a ferron ground state, in which five neighboring copper ions all have parallel spins.

The mean field methods used here are therefore expected to yield a good description of systems where fluctuations such as polaron hopping or stripe fluctuation are relatively unimportant. Incorporation of such effects is not yet possible in *ab initio* electronic structure methods. However, even for systems where such fluctuations are important, the calculations presented above reveal important configurations in any ensemble observed in experiment.

### B. Low hole-density limit

Experimental evidence for localized, polaronic hole states at low doping levels in cuprates comes from the frequency dependence of the dielectric constant and conductivity[56] and

optical excitation of impurities[47] in $La_2CuO_{4+y}$, with $y$ in the range 0.0001–0.01 and optical excitation data for a range of low hole-doped cuprates.[57] The binding energy of the hole to interstitial oxygen ions in $La_2CuO_{4+y}$ was determined to be 35 meV from Hall measurements.[56] A power-law dependence of conductivity on frequency was ascribed to thermally assisted tunneling between localized states.[56] Several broad absorption features in the midinfrared have been reported for a number of low doped cuprates[47,57] and have been successfully modeled as small polarons bound to impurities.[58] A combined NMR and NQR study of $La_2CuO_{4+y}$ with $y$ in the range 0.06–0.12,[59] showed that an additional line in the copper NQR spectrum of $La_2CuO_{4+y}$ could be assigned to a hole pinned to the lattice.

In this paper, we have shown that holes in Na-CCOC form small polarons which form preferentially adjacent to sodium impurities at low hole concentration. The spatial extent of the polaron is approximately $2a_0$ by inspection of dispersionless occupied and vacant states (Fig. 2) associated with the polaron. Inclusion of nonlocal Hartree–Fock exchange in the Hamiltonian is partly responsible for localization of the hole, as demonstrated by a threshold for formation of small polarons which lies between $A=0.2$ and 0.3 when a hole is introduced by removing an electron from the unit cell and replacing it by a uniform background charge. However, the important role of dopant sodium ions in polaron formation is demonstrated by ready formation of small polarons adjacent to the dopant ion when $A=0.2$. Localization of holes in calculations where nonlocal Hartree–Fock exchange is included, for lattices where the periodicity is not broken, has been demonstrated for a number of systems including $Sr_2CuO_3$,[60] $La_{0.5}Ca_{0.5}MnO_3$,[8] and $Sr_2CuO_2Cl_2$.[61] Relaxation of the lattice when a localized hole is present results in a significant contraction (4%) of Cu-O bond lengths about the central copper ion. Small polarons with similar contractions of four oxygen ions around the central copper ion in the polaron have been found using quantum chemical methods applied to clusters.[11] Recently, Gunnarsson *et al.*[62] demonstrated that electron-phonon coupling in cuprates is sufficiently strong for small polaron formation. We have not considered such dynamical electron-phonon interaction effects here and these may further stabilize polaron formation.

The Zhang–Rice singlet state[12] and Emery–Reiter spin polaron[13] are models for holes in cuprates, which were proposed not long after the discovery of cuprate superconductivity. The ground state for a hole in the Zhang–Rice model consists of an electron in a linear combination of O $2p\sigma$ states around one copper ion with opposite spin to the $d_{x^2-y^2}$ electron on the copper ion with an open-shell singlet coupling of those spins. A key aspect of the Zhang–Rice singlet model is that holes in cuprates can be mapped onto a one-band Hubbard model on copper sites. The Emery–Reiter ground state[13] can be written as a linear superposition of singlet states, in which the spins on neighboring copper ions are *parallel*, the spin of the oxygen ion is antiparallel to the copper spins, and there is a net magnetic moment of $-\mu_B/3$ on the oxygen ion. These solutions to model Hamiltonians are composed of more than one configuration, whereas the first principles approach used here uses a single self-consistent field configuration. Hence, spin fluctuations such as those incorporated in the Zhang–Rice and Emery–Reiter models are omitted. In common with the Emery–Reiter model, we find that the state with the central copper ion spin parallel to spins of neighboring copper spins is energetically favored over a polaron where the central copper spin is antiparallel to the neighboring copper spins. The energy difference is several tenths of an eV.

For the small polaron state, we find that the magnetic moment on the central copper ion is significantly smaller than that on the other copper ions in the $Cu_5O_4$ polaron unit (by around 30% for a polaron generated by substituting a calcium ion and by 20% by removing an electron according to Table I). Inspection of wave function coefficients for the states in the band gap formed by the small polaron (Fig. 2) shows that the hole is predominantly localized on the central copper ion; the combined weights for the hole on the four oxygen ions in the polaron amount to 30%–40% and most of the remainder is on the central copper ion. This observation accounts for the reduced magnetic moment on the copper ion.

The magnetic phase diagram of $Ca_{2-x}Na_xCuO_2Cl_2$ has been determined by muon spin resonance.[52] The antiferromagnetic insulating state of the parent compound vanishes beyond a hole concentration of 0.02 and is replaced by a spin glass state in the range $0.02<x<0.12$. Superconductivity first appears around $x=0.10$ and the volume fraction of the superconducting phase is maximal (60%) at $x=0.15$. Fast relaxation of the muon spin polarization without any detectable oscillation was observed for $x=0.05$ and was attributed to disordered magnetism.[52] We have shown that relative Coulomb repulsion energies of small polarons which are next to each other in this hole concentration range ($x=0.0625$) in the absence of lattice relaxation are of order 350 meV. Since lattice relaxation effects will reduce this repulsion energy, the energy which may dominate the sites on which polarons localize may be the binding energy to the impurity.

### C. Stripe and checkerboard hole density

$La_{2-x}Ba_xCuO_4$,[34,53,63] $YBaCuO_{6+\delta}$,[28] $La_{1.28}Nd_{0.6}Sr_{0.12}CuO_4$,[64,65] and $La_{1.85}Sr_{0.15}CuO_4$ (Ref. 65) are systems in which charge stripes have definitely been observed by magnetic[28,34,53] and phonon[34] inelastic neutron scatterings, photoemission,[64,65] and resonant x-ray scattering.[63] Scanning tunneling spectroscopy on $Ca_{2-x}Na_xCuO_2Cl_2$ with $0.08\leqslant x\leqslant 0.12$ has revealed a $4\times4$ checkerboard pattern[24] and 1D stripes.[25] However, a recent resonant x-ray scattering study of $Ca_{2-x}Na_xCuO_2Cl_2$, with $x=0.08$,[66] failed to find a $4\times4$ modulation of the density of states, whereas an earlier similar study of $La_{1.88}Ba_{0.12}CuO_4$ (Ref. 63) did show static charge order. A three-band, $t$-$t'$-$U$, Hubbard model study of the $CuO_2$ plane, where the ratio of $|t'/t|$ was varied, found stripes or checkerboards to be stabilized for different values of this parameter at doping levels $x=0.06$ or 0.125.[67] The authors of that study concluded that 1D stripes separated by $4a_0$ are favored when the ratio $|t'/t|$ is relatively small (0.2) but that checkerboards are favored when this ratio is large (0.5). Inspection of the lower right panel of Fig. 8 shows that holes in the $4\times4$ checkerboard

state studied in this work are mainly localized on quadruples of copper ions at stripe intersections. In contrast to the small polaron state in Fig. 2, the hole density is predominantly on oxygen sites rather than the copper site at the center of the small polaron. Hole density in our checkerboard calculation, judged by distribution of wave function amplitude for the vacant state in the gap in Fig. 8, most closely resembles the small ferron checkerboard shown in Figs. 1(b) and 1(c) of Ref. 67. Seibold *et al.*[67] concluded that the known value of $|t'/t|$ for Na-CCOC places it close to the phase stability boundary between stripes and checkerboards.

A peak identified as a mobile carrier peak which lies around 2 eV below the upper Hubbard band peak is a common feature of resonant x-ray scattering experiments. This peak is found in $La_{1.85}Sr_{0.15}CuO_4$,[68] $La_{1.88}Ba_{0.12}CuO_4$,[63] and $Ca_{1.88}Na_{0.12}CuO_2Cl_2$ (Ref. 66) and is absent from undoped $La_2CuO_4$.[68] It seems likely that the dispersionless state found in the checkerboard band structure around 2 eV below the vacant $d_{x^2-y^2}$ states in Fig. 9 is the state responsible for the mobile carrier peak.

In a three-band Hubbard model for a 1D stripe,[69] the weight of holes projected onto oxygen ions in the $CuO_2$ plane was greatest (0.121) on the O $2p\sigma$ state on oxygen ions bonded to copper ions in the stripe which are "legs" rather than "rungs" of the stripe ladder. The weight of holes on rungs was next greatest (0.095) and the weight on oxygen ions midway between stripes was 0.034. An LDA+$U$ calculation[10] on $La_{1.88}Sr_{0.12}CuO_4$ found holes on copper ions in the stripe to have the greatest weight (0.076), while holes on rungs of the stripe ladder had weight 0.066 and holes on legs of the stripe ladder had significantly smaller weight. As noted above, the distribution of wave function amplitude in the stripe band shown in the bottom panel of Fig. 6 is similar to the Wannier function for the stripe band in the LDA+$U$ calculation just mentioned. Inspection of Fig. 6 shows that hole amplitude is mainly localized on oxygen ions in rungs of the stripe and that there is also large amplitude for the hole on the copper ions in the stripe.

We now make a comparison between the shape of the Fermi surface predicted by hybrid DFT calculations, an LDA+$U$ calculation[10] and experiment. The hybrid DFT band structure for the $8\times2$ supercell in Fig. 7 shows four stripe localized bands with a bandwidth of approximately 600 meV and the Fermi level falling roughly in the middle of the band at $|k|=\pi/4$. There is little dispersion of these bands in a direction perpendicular to the stripes, whereas there is some dispersion of the bands perpendicular to the stripes in the LDA+$U$ calculation of Anisimov *et al.*[10] The shape of the Fermi surface predicted for 1D stripes by these calculations is therefore a pair of parallel lines (hybrid DFT calculation on $Ca_{1.88}Na_{0.12}CuO_2Cl_2$) or a slightly wavy pair of nearly parallel lines (LDA+$U$ calculation on $La_{1.88}Sr_{0.12}CuO_4$) in $k$ space, perpendicular to the stripe direction; the component of the Fermi wave vector parallel to the stripes is approximately $\pm\pi/4$.

Photoemission studies of $La_{1.28}Nd_{0.6}Sr_{0.12}CuO_4$ and $La_{1.85}Sr_{0.15}CuO_4$,[64,65] in which photoemission intensity was integrated in a window within several hundred meV of the Fermi level, found that this intensity was sharply confined within a pair of bands in a cross shape where $|k_x|$ or $|k_y|$ $<\pi/4$. This pattern of photoemission is consistent with the electronic structure found in the stripe calculations in Figs. 6 and 7. The cross shape is expected to arise from two domain orientations of the stripes.

Photoemission studies of $Ca_{2-x}Na_xCuO_2Cl_2$,[70,71] with $x=0.12$, obtained the Fermi surface, but integration of photoemission intensity in a window close to the Fermi level was not reported. The Fermi surface consists of half-moon regions at 45° to the Cu-O bond directions, which are quite distinct from the perpendicular stripe photoemission intensity distribution reported for $La_{1.28}Nd_{0.6}Sr_{0.12}CuO_4$ or $La_{1.85}Sr_{0.15}CuO_4$. However, $La_{1.88}Ba_{0.12}CuO_4$, which is known to form statically ordered stripes, has a Fermi surface,[72] which is quite similar to that of $Ca_{1.88}Na_{0.12}CuO_2Cl_2$.

## VII. SUMMARY

Hybrid DFT calculations on $Ca_{2-x}Na_xCuO_2Cl_2$, with $x=0.0625$, in $4\times4$ supercells result in small polaron wave functions where the hole is localized on one $Cu_5O_4$ unit. All copper ions in the polaron are ferromagnetically coupled. The formation of this small polaron is accompanied by appearance of a localized occupied minority spin state less than 0.5 eV below the valence band maximum. Localized, empty majority and minority spin states appear in the band gap when the polaron forms. Holes in these calculations were generated either by removing one electron from the unit cell and replacing it by a uniform, neutralizing background charge or by replacing one calcium ion by a sodium ion. In the former case, the spin density on the polaron has a fourfold symmetry and oxygen ions in the small polaron have opposite net magnetic moments to those of the copper ions in the polaron. However, when a hole is generated by replacing a calcium ion, the polaron forms on a $Cu_5O_4$ unit adjacent to the sodium ion and the net magnetic moment on the oxygen ions has the same sense as the copper ions in the polaron. Inspite of this difference in net magnetic moment on oxygen ions in the polaron, the localized states associated with the polaron are very similar and are therefore independent of the means of generating the hole. Pairs of polarons in a $4\times4$ supercell have purely repulsive interactions, which can be characterized as a screened Coulomb potential with dielectric constant $\epsilon_\infty=5$.

The picture of stripe order in cuprates which emerges from these calculations is one where holes are largely confined to magnetic antiphase boundaries (stripes) which separate regions where spins of copper ions are ordered antiferromagnetically, either in long blocks which may contain $4\times\sim10$ copper ions in 1D stripes[25] or in $4\times4$ blocks in tiles.[24] Magnetic moments of copper ions in these striped phases are close to their values in the antiferromagnetic insulating parent compound and there is a small magnetic moment on oxygen ions within stripes. A group of half-filled bands is predominantly localized on Cu-O-Cu units in the stripe which makes antiphase boundaries metallic. Regions between them remain insulating. These linear, metallic stripes are likely to be the origin of 1D stripes in $Ca_{2-x}Na_xCuO_2Cl_2$ observed by STM.[25] Hybrid DFT calcula-

tions on $Ca_{2-x}Na_xCuO_2Cl_2$, with $x=1/8$, with intersecting antiphase boundaries separated by four lattice constants also result in an electronic structure where wave functions are localized on Cu-O-Cu units. These may be the origin of the $4\times4$ phase in earlier reports of STM conductance maps.[24]

## ACKNOWLEDGMENTS

This work was supported by the Irish Higher Education Authority (IHEA) under the PRTLI-III program IITAC-II. Computer time was provided by the Trinity Centre for High Performance Computing which is supported under the Irish National Development Plan. The author wishes to acknowledge helpful discussions with J. C. Davis and Y. Kohsaka.

## APPENDIX: DETAILS OF CALCULATIONS

Hybrid DFT calculations were performed using the CRYSTAL program.[73] Spin density plots were generated using the XCRYSDEN program.[74,75] Gaussian orbital basis sets were standard all electron basis sets for Na,[76] Ca,[77] Cu,[78] O,[79] and Cl.[80] The Cu basis was supplemented by an extra *d* orbital with an exponent of 0.20 $Bohr^{-2}$ and the outer exponent of the standard Cu basis[78] was adjusted to 0.43 $Bohr^{-2}$. The outer *sp* exponents of the Cl basis were modified to 0.294 and 0.090 $Bohr^{-2}$. Tolerances for lattice sum convergence within the CRYSTAL program were chosen to be 7 7 7 7 14.

Calculations were performed using the $P_m$ space group symmetry with the mirror plane parallel to $CuO_2$ planes. Under this space group, *all* copper and oxygen ions are unique and Cl and Ca ions are equivalent in pairs. The use of a much lower symmetry than is present in undoped parent compounds is important as low energy localized polaronic states tend to break that high symmetry. Localization of holes is observable either from total charges and magnetic moments projected onto sites in Mulliken population analyses or by plotting the total spin density. In the latter case, hole density is apparent because of uncompensated spin of the remaining electron on the site where the hole is localized.

[1] J. S. Zhou and J. B. Goodenough, Phys. Rev. B **56**, 6288 (1997).
[2] L. Perfetti, S. Mitrovic, G. Margaritondo, M. Grioni, L. Forró, L. Degiorgi, and H. Höchst, Phys. Rev. B **66**, 075107 (2002).
[3] K. M. Shen *et al.*, Phys. Rev. Lett. **93**, 267002 (2004).
[4] H. M. Ronnow, C. Renner, G. Aeppli, T. Kimura, and Y. Tokura, Nature (London) **440**, 1025 (2006).
[5] S. Raj, D. Hashimoto, H. Matsui, S. Souma, T. Sato, T. Takahashi, D. D. Sarma, P. Mahadevan, and S. Oishi, Phys. Rev. Lett. **96**, 147603 (2006).
[6] K. M. Shen *et al.*, Phys. Rev. B **75**, 075115 (2007).
[7] S. Grenier *et al.*, Phys. Rev. Lett. **99**, 206403 (2007).
[8] G. Zheng and C. H. Patterson, Phys. Rev. B **67**, 220404(R) (2003).
[9] V. Ferrari, M. Towler, and P. B. Littlewood, Phys. Rev. Lett. **91**, 227202 (2003).
[10] V. I. Anisimov, M. A. Korotin, A. S. Mylnikova, A. V. Kozhevnikov, D. M. Korotin, and J. Lorenzana, Phys. Rev. B **70**, 172501 (2004).
[11] L. Hozoi, S. Nishimoto, G. Kalosakas, D. B. Bodea, and S. Burdin, Phys. Rev. B **75**, 024517 (2007).
[12] F. C. Zhang and T. M. Rice, Phys. Rev. B **37**, 3759 (1988).
[13] V. J. Emery and G. Reiter, Phys. Rev. B **38**, 4547 (1988).
[14] L. F. Mattheiss, Phys. Rev. B **42**, 354 (1990).
[15] D. J. Singh and W. E. Pickett, Phys. Rev. B **44**, 7715 (1991).
[16] J. Lorenzana and G. Seibold, Low Temp. Phys. **32**, 320 (2006).
[17] D. Poilblanc and T. M. Rice, Phys. Rev. B **39**, 9749 (1989).
[18] J. Zaanen and O. Gunnarsson, Phys. Rev. B **40**, 7391 (1989).
[19] H. J. Schulz, J. Phys. (Paris) **50**, 2833 (1989).
[20] A. D. Becke, J. Chem. Phys. **98**, 5648 (1993).
[21] P. J. Stephens, F. J. Devlin, C. F. Chabalowski, and M. J. Frisch, J. Phys. Chem. **98**, 11623 (1994).
[22] C. H. Patterson, Mol. Phys. **103**, 2507 (2005).
[23] C. H. Patterson, Phys. Rev. B **77**, 115111 (2008).
[24] T. Hanaguri, C. Lupien, Y. Kohsaka, D.-H. Lee, M. Azuma, M. Takano, H. Takagi, and J. C. Davis, Nature (London) **430**, 1001 (2004).
[25] Y. Kohsaka *et al.*, Science **315**, 1380 (2007).
[26] J. M. Tranquada, B. J. Sternlieb, J. D. Axe, Y. Nakamura, and S. Uchida, Nature (London) **375**, 561 (1995).
[27] J. M. Tranquada, N. Ichikawa, and S. Uchida, Phys. Rev. B **59**, 14712 (1999).
[28] S. M. Hayden, H. A. Mook, P. Dai, T. G. Perring, and F. Dogan, Nature (London) **429**, 531 (2004).
[29] J. Haase, C. P. Slichter, R. Stern, C. T. Milling, and D. Hinks, Physica C **341-348**, 1727 (2000).
[30] J. Haase, C. P. Slichter, and C. T. Milling, J. Supercond. **15**, 339 (2002).
[31] S. A. Kivelson, I. P. Bindloss, E. Fradkin, V. Oganesyan, J. M. Tranquada, A. Kapitulnik, and C. Howal, Rev. Mod. Phys. **75**, 1201 (2003).
[32] J. P. Falck, A. Levy, M. A. Kastner, and R. J. Birgeneau, Phys. Rev. Lett. **69**, 1109 (1992).
[33] X.-X. Bi and P. C. Eklund, Phys. Rev. Lett. **70**, 2625 (1993).
[34] D. Reznik, L. Pintschovius, M. Ito, S. Iikubo, M. Sato, H. Goka, M. Fujita, K. Yamada, G. D. Gu, and J. M. Tranquada, Nature (London) **440**, 1170 (2006).
[35] R. L. Martin and F. Illas, Phys. Rev. Lett. **79**, 1539 (1997).
[36] J. K. Perry, J. Tahir-Kheli, and W. A. Goddard, Phys. Rev. B **63**, 144510 (2001).
[37] X. Feng, J. Phys.: Condens. Matter **16**, 4251 (2004).
[38] I. D. R. Moreira and R. Dovesi, Int. J. Quantum Chem. **99**, 805 (2004).
[39] F. Cora, M. Alfredsson, G. Mallia, D. Middlemiss, W. C. Mackrodt, R. Dovesi, and R. Orlando, Struct. Bonding (Berlin) **113**, 171 (2004).
[40] C. H. Patterson, Int. J. Quantum Chem. **106**, 3383 (2006).
[41] C. H. Patterson, Phys. Rev. B **74**, 144432 (2006).
[42] P. A. M. Dirac, Proc. Cambridge Philos. Soc. **26**, 376 (1930).
[43] A. D. Becke, Phys. Rev. A **38**, 3098 (1988).
[44] C. Lee, W. Yang, and R. G. Parr, Phys. Rev. B **37**, 785 (1988).

[45] S. H. Vosko, L. Wilk, and M. Nusair, Can. J. Phys. **58**, 1200 (1980).
[46] L. Hedin, Phys. Rev. **139**, A796 (1965).
[47] J. P. Falck, A. Levy, M. A. Kastner, and R. J. Birgeneau, Phys. Rev. B **48**, 4043 (1993).
[48] J. L. Gavartin, P. V. Sushko, and A. L. Shluger, Phys. Rev. B **67**, 035108 (2003).
[49] P. G. Radaelli, D. E. Cox, M. Marezio, and S.-W. Cheong, Phys. Rev. B **55**, 3015 (1997).
[50] C. H. Patterson, Phys. Rev. B **72**, 085125 (2005).
[51] C. Y. Chen, N. W. Preyer, P. J. Picone, M. A. Kastner, H. P. Jenssen, D. R. Gabbe, A. Cassanho, and R. J. Birgeneau, Phys. Rev. Lett. **63**, 2307 (1989).
[52] K. Ohishi, I. Yamada, A. Koda, W. Higemoto, S. R. Saha, R. Kadono, K. M. Kojima, M. Azuma, and M. Takano, J. Phys. Soc. Jpn. **74**, 2408 (2005).
[53] J. M. Tranquada, H. Woo, T. G. Perring, H. Goka, G. D. Gu, G. Xu, M. Fujita, and K. Yamada, Nature (London) **429**, 534 (2004).
[54] R. Coldea, S. M. Hayden, G. Aeppli, T. G. Perring, C. D. Frost, T. E. Mason, S.-W. Cheong, and Z. Fisk, Phys. Rev. Lett. **86**, 5377 (2001).
[55] D. C. Peets, J. D. F. Mottershead, B. Wu, I. S. Elfimov, R. Liang, W. N. Hardy, D. A. Bonn, M. Raudsepp, N. J. C. Ingle, and A. Damascelli, New J. Phys. **9**, 28 (2007).
[56] C. Y. Chen, R. J. Birgeneau, M. A. Kastner, N. W. Preyer, and T. Thio, Phys. Rev. B **43**, 392 (1991).
[57] G. A. Thomas, D. H. Rapkine, S. L. Cooper, S.-W. Cheong, A. S. Cooper, L. F. Schneemeyer, and J. V. Waszczak, Phys. Rev. B **45**, 2474 (1992).
[58] M. A. Kastner, R. J. Birgeneau, G. Shirane, and Y. Endoh, Rev. Mod. Phys. **70**, 897 (1998).
[59] P. C. Hammel, B. W. Statt, R. L. Martin, F. C. Chou, D. C. Johnston, and S.-W. Cheong, Phys. Rev. B **57**, R712 (1998).
[60] W. C. Mackrodt and H. J. Gotsis, Phys. Rev. B **62**, 10728 (2000).
[61] D. S. Middlemiss and W. C. Mackrodt, J. Phys.: Condens. Matter **20**, 15207 (2008).
[62] O. Gunnarsson, G. Sangiovannia, O. Röscha, E. Koch, C. Castellani, and M. Capone, Physica C **460**, 263 (2007).
[63] P. Abbamonte, A. Rusydi, S. Smadici, G. D. Gu, G. A. Sawatzky, and D. L. Feng, Nat. Phys. **1**, 155 (2005).
[64] X. J. Zhou, P. Bogdanov, S. A. Kellar, T. Noda, H. Eisaki, S. Uchida, Z. Hussain, and Z.-X. Shen, Science **286**, 268 (1999).
[65] X. J. Zhou *et al.*, Phys. Rev. Lett. **86**, 5578 (2001).
[66] S. Smadici, P. Abbamonte, M. Taguchi, Y. Kohsaka, T. Sasagawa, M. Azuma, M. Takano, and H. Takagi, Phys. Rev. B **75**, 075104 (2007).
[67] G. Seibold, J. Lorenzana, and M. Grilli, Phys. Rev. B **75**, 100505(R) (2007).
[68] C. T. Chen, L. H. Tjeng, J. Kwo, H. L. Kao, P. Rudolf, F. Sette, and R. M. Fleming, Phys. Rev. Lett. **68**, 2543 (1992).
[69] J. Lorenzana and G. Seibold, Phys. Rev. Lett. **89**, 136401 (2002).
[70] F. Ronning *et al.*, Phys. Rev. B **67**, 165101 (2003).
[71] K. M. Shen *et al.*, Science **307**, 901 (2005).
[72] T. Valla, A. V. Fedorov, J. Lee, J. C. Davis, and G. D. Gu, Science **314**, 1914 (2006).
[73] R. Dovesi *et al.*, *Crystal06 User's Manual* (University of Torino, Torino, 2007).
[74] A. Kokalj, Comput. Mater. Sci. **28**, 155 (2003).
[75] Code available from http://www.xcrysden.org
[76] R. Dovesi, C. Roetti, C. Freyria-Fava, M. Prencipe, and V. Saunders, Chem. Phys. **156**, 11 (1991).
[77] W. C. Mackrodt, Philos. Mag. A **68**, 653 (1993).
[78] K. Doll and N. M. Harrison, Chem. Phys. Lett. **317**, 282 (2000).
[79] M. D. Towler, N. L. Allan, N. M. Harrison, V. R. Saunders, W. C. Mackrodt, and E. Aprà, Phys. Rev. B **50**, 5041 (1994).
[80] E. Apra, M. Causa, M. Prencipe, R. Dovesi, and V. Saunders, J. Phys.: Condens. Matter **5**, 2969 (1993).